Mass Transport Mechanism of Cu Species at the Metal/Dielectric Interfaces with a Graphene Barrier

Yuda Zhao,[†,‡] Zhaojun Liu,[§,∥] Tieyu Sun,[†] Ling Zhang,[†] Wenjing Jie,[†] Xinsheng Wang,[†] Yizhu Xie,[†] Yuen Hong Tsang,[†] Hui Long,[†] and Yang Chai*,[†,‡]

[†]Department of Applied Physics, The Hong Kong Polytechnic University, Hung Hom, Kowloon, Hong Kong, People's Republic of China, [‡]Shenzhen Research Institute, The Hong Kong Polytechnic University, Shenzhen, People's Republic of China, [§]SYSU-CMU Joint Institute of Engineering, Sun Yat-sen University, Guangdong, People's Republic of China, and [∥]SYSU-CMU Shunde International Joint Research Institute, Shunde, Guangdong, People's Republic of China

ABSTRACT The interface between the metal and dielectric is an indispensable part in various electronic devices. The migration of metallic species into the dielectric can adversely affect the reliability of the insulating dielectric and can also form a functional solid-state electrolyte device. In this work, we insert graphene between Cu and SiO_2 as a barrier layer and investigate the mass transport mechanism of Cu species through the graphene barrier using density functional theory calculations, second-ion mass spectroscopy (SIMS), capacitance–voltage measurement, and cyclic voltammetry. Our theoretical calculations suggest that the major migration path for Cu species to penetrate through the multiple-layered graphene is the overlapped defects larger than 0.25 nm^2. The depth-profile SIMS characterizations indicate that the "critical" thickness of the graphene barrier for completely blocking the Cu migration is 5 times smaller than that of the conventional TaN barrier. Capacitance–voltage and cyclic voltammetry measurement reveal that the electrochemical reactions at the Cu/SiO_2 interface become a rate-limiting factor during the bias-temperature stressing process with the use of a graphene barrier. These studies provide a distinct roadmap for designing controllable mass transport in solid-state electrolyte devices with the use of a graphene barrier.

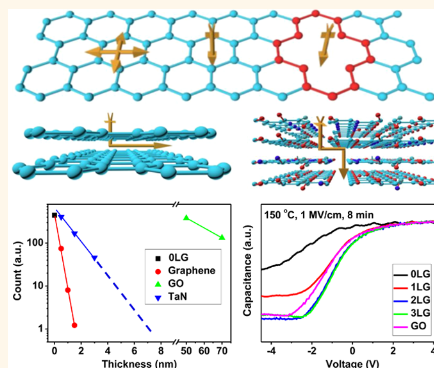

KEYWORDS: Cu interconnect · barrier · mass transport · graphene

Metallic species migration (atom diffusion and ion drift) through the metal/dielectric interfaces and the chemical reaction between the metal and dielectrics significantly affect the performance and reliability of electronic devices. The intrinsic complexity of the metal/dielectric interface is caused by the interdiffusion and is further complicated by the electrical/thermal stress that usually occurs in electronic devices. As the feature size of the integrated circuit technology continues to scale downward toward the nanoscale, the state-of-the-art Cu/low-*k* interconnect technology faces a number of challenges, including the increasing resistivity and poor electromigration resistance.[1−6] A thin barrier layer is used between the Cu conductor and the surrounding dielectrics to prevent Cu species from diffusing into dielectrics. According to the International Technology Roadmap for Semiconductors in 2011, the thickness of the barrier layer for the Cu interconnect is projected to be less than 1 nm by 2021. It has been expected that the TaN/Ta barrier material will fail at such a small dimension.[7,8] To enable continuous downward scaling of the Cu interconnect, researchers must develop an ultrathin layer (<1 nm) with high resistance to Cu species migration inside low-*k* dielectrics.

The intrinsic "pore" size (0.064 nm) of the hexagonal lattice in graphene is smaller than the van der Waals radii of the smallest molecules and atoms, leading to high impermeability of the graphene nanosheet.[9−11] Highly impermeable graphene has been demonstrated for impeding the migration of liquid, gas, and chemical/biological molecules.[12−17] Recently, researchers used a graphene layer for preventing the reaction and interdiffusion at the interfaces of Al/Si, Cu/Si, and Au/Ni.[18−20] These results indicate the possibility of introducing a graphene barrier

* Address correspondence to ychai@polyu.edu.hk.

Received for review September 27, 2014 and accepted November 25, 2014.

Published online November 25, 2014
10.1021/nn5054987

© 2014 American Chemical Society

into solid-state electrolyte devices, *e.g.*, the controllable mass transport in electrochemical metalization memory cells.[21,22] In order to further improve the barrier performance close to practical applications, researchers must understand the mass transport mechanism at the metal/dielectric interface with a graphene barrier.

First, it is important to investigate the migration paths of the metal species through the graphene barrier at the metal/dielectric interfaces and design the barrier structure to minimize the metal species migration. Second, the properties of graphene and a conventional TaN barrier have not been quantitatively compared in terms of thickness, barrier performance, and sheet resistance. Third, during the electrical stressing in electronic devices, the metal species migration is dominated by the metal ion drift driven by the electric field, where the metal ions are intrinsically generated by the electrochemical reaction at the metal/dielectric interface. The generation of the metal ions at the metal/dielectric interfaces with a graphene barrier is still unclear. Fourth, the drift kinetics of the metal ion under electrical stressing determines the total amount and distribution of the metal ions in the dielectrics. These factors are crucial for predicating the dielectrics' reliability. In this work, we theoretically investigate the migration paths of metal species in multiple-layered graphene (MLG) using density functional theory (DFT) calculations. We also experimentally study the effects of the graphene barrier on the atomic diffusion, ionic drift, and electrochemical reaction at the interface and monitor the Cu ion drift using the capacitance−voltage characterization.

RESULTS AND DISCUSSION

Intrinsic defects and grain boundary inevitably exist in graphene grown by the chemical vapor deposition (CVD) method. These defects and grain boundaries can be further enlarged during the transfer process and the subsequent treatment. In order to completely impede the atom/molecule migration through these defects, researchers have adopted MLG to cover the intrinsic defects of the graphene.[23,24] In the barrier structure with MLG at the metal/dielectric interface, there are five possible migration paths for the metal species: (1) along the basal plane of graphene; perpendicular to the basal plane of graphene (2) without defects and (3) with defects; (4) migration between two graphene layers; and (5) perpendicular to the edge plane of graphene, as depicted in Figure 1A.

DFT Calculations. We first conducted DFT studies to calculate the barrier potential for each possible path and unravel the migration route of the Cu species through the graphene barrier. The inset of Figure 1B shows the schematics of the interaction between a Cu atom and different sites (top, bridge, and hollow) of graphene. We calculated the adsorption energy between the Cu atom and different sites of graphene using the DFT method.[25] The adsorption energy between the Cu atom and the bridge site of graphene is −1.19 eV, the highest one among the three sites. The adsorption energies between the Cu atom and the hollow and top sites of graphene are −0.86 and −1.13 eV, respectively. The interaction between the Cu atom and the graphene surface is weak, and the adsorption energy differences at different adsorption sites are insignificant, allowing Cu atoms to freely migrate on the surface of graphene.

When we force a Cu atom to perpendicularly pass through the basal plane of a perfect graphene lattice, the dense electron clouds of the graphene repel the translocation of the Cu atom. Our DFT calculation results demonstrate that the potential barrier for the Cu atom translocation through the graphene basal plane is as large as 30.62 eV, as shown in Figure 1C. This extremely high barrier potential prohibits the passage of Cu species, indicating that the perfect graphene layer is highly impermeable to the migration of Cu species. These results also suggest that the migration paths of the Cu atom on the graphene surface are highly anisotropic: free movement on the surface of graphene but complete blockage through the basal plane of graphene.

We further calculated the interaction between a Cu atom and the nanoscale defective sites in the graphene. At the monovacancy site of graphene, a Cu atom is adsorbed on the graphene surface with a 0.1 nm distance. The adsorption energy is calculated to be −7.32 eV. The adsorption of a Cu species at the defective site of the graphene layer is energetically favorable. As shown in Figure 1D, when a Cu atom passes through the monovacancy of single-layer graphene, the potential barrier is quite high (6.44 eV) due to the steric hindrance effect, where the vacancy is too small for a Cu atom to pass through. Figure 1E shows the potential barrier for the Cu atom migration through graphene with divacancy and eight-atom vacancy. For the divacancy site, the adsorption energy is −11.70 eV. The energy valley at the divacancy site is very sharp, and the Cu atom has been trapped in the defect. We further enlarge the defective site to an eight-atom vacancy (0.25 nm^2) and find that the adsorption energy of the Cu atom in the defective center decreases to −3.40 eV. The Cu atom can still adsorb at the center of the vacancy, but the energy valley is flat, which allows the Cu atom to penetrate through the basal plane of the graphene. These results showed that the barrier potential for Cu species to penetrate through the basal plane of graphene decreases with the increase of the defect size.

In the MLG barrier structure, the interlayer space provides another possible migration path for Cu species. We used A−B stacked bilayer graphene (interlayer distance is 0.334 nm) with mismatched defects as a

VOL. 8 ▪ NO. 12 ▪ 12601–12611 ▪ 2014 ACSNANO www.acsnano.org

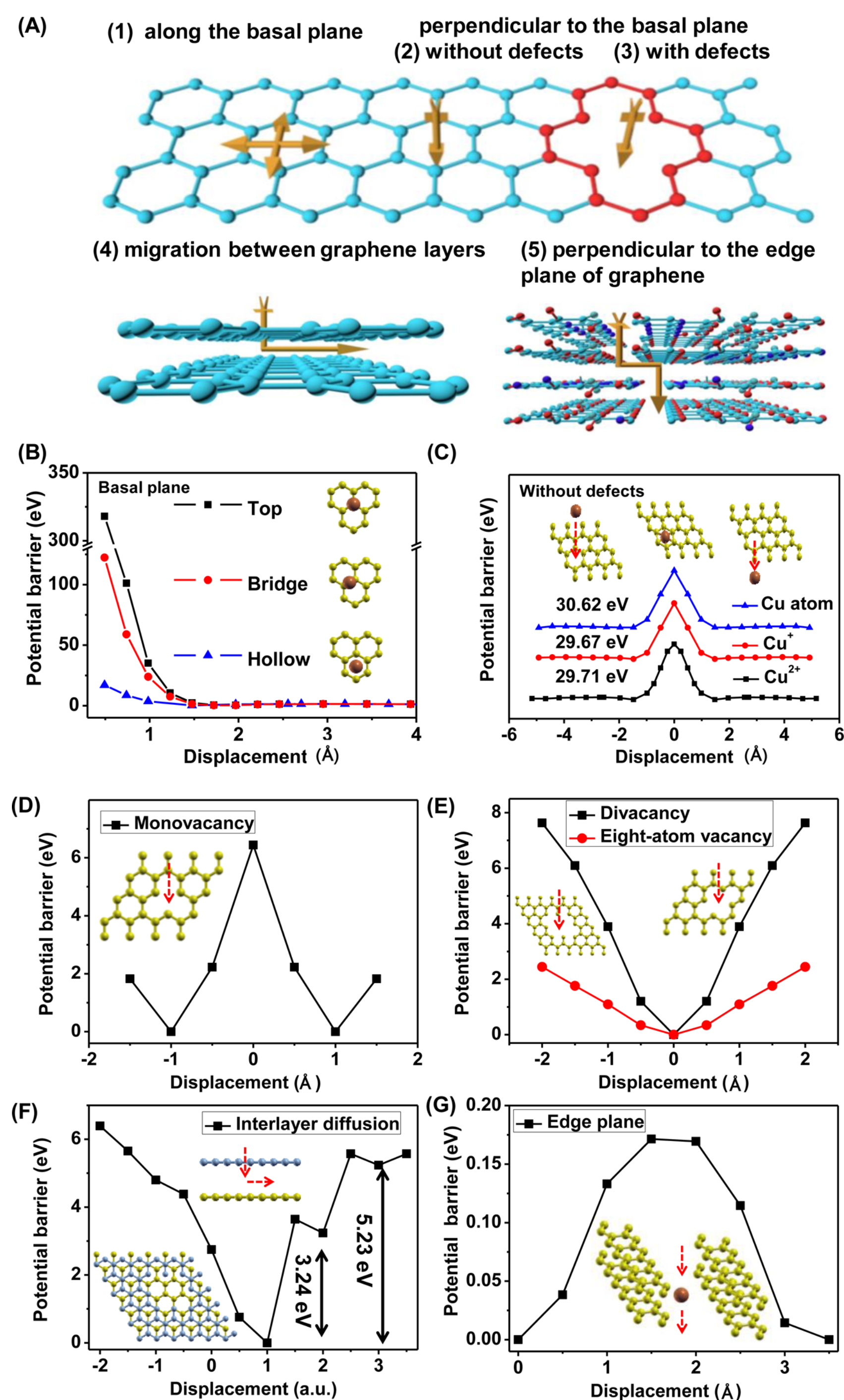

Figure 1. DFT calculations of the Cu species migration through a graphene barrier. (A) Schematics of five possible migration paths of Cu species at a graphene barrier. (B) Translocation potential barrier of Cu atoms adsorbed at top, bridge, and hollow sites. (C) Potential barrier of different Cu species through the hollow of the graphene lattice. (D) Potential barrier of Cu atom diffusion through a monovacancy site of graphene. (E) Potential barrier for a Cu atom passing through the divacancy and eight-atom vacancy defects. (F) Potential barrier of a Cu atom permeating into the interlayer of double-layer graphene. (G) Potential barrier of Cu atom diffusion perpendicular to the edge plane. The arrows indicate the migration direction of the Cu species.

representative to investigate the migration of Cu species, as shown in Figure 1F. When we force a Cu atom to penetrate through the center of an eight-atom vacancy, it adsorbs at the top graphene layer and diffuses to the edge of the defect. Translocating into the interlayer requires the Cu atom to overcome a potential barrier as high as 5.23 eV. This relatively large potential barrier makes the migration of Cu species between two graphene layers (with a 0.334 nm distance) less likely to happen.

The edge plane of graphene can be regarded as a defective site much larger than the eight-atom vacancy.

We estimate the potential barrier for the edge plane migration by forcing a Cu atom to pass through the zigzag edge of double-layer graphene, as shown in Figure 1G. The potential barrier is 0.17 eV, showing weak interaction between the Cu atom and the edge plane of the graphene. Cu atoms can easily diffuse perpendicular to the edge plane. These results also indicate that the MLG with overlapped defects exhibits inferior performance. Graphene oxide (GO) has a similar atomic structure to that of pristine graphene and has been also demonstrated with high impermeability.[26−28] The GO flakes are relatively small and have many edge planes, providing a platform for studying Cu migration through the edge plane of graphene.

Thermal Stress. Nguyen *et al*. and Hong *et al*. have successfully evaluated the graphene barrier properties between Cu and Si, where a few-nanometer native SiO_2 exists on top of the Si.[19,20] In order to accurately characterize the barrier properties close to the real interconnect structure, we grew a 100 nm thick thermal SiO_2 on an n-type Si (100) wafer instead of using a native SiO_2 layer. Figure 2A shows a schematic drawing of the test structure, where Cu was deposited onto the SiO_2 thin film. A graphene barrier is sandwiched between Cu and SiO_2. The barrier layer includes single-, double-, and triple-layer graphene and tens of layers graphene oxide (denoted as 1LG, 2LG, 3LG, GO). The sample without a barrier layer was fabricated as a control structure (denoted as 0LG). Figure 2B shows a cross-sectional scanning electron microscopy (SEM) image of a Cu/graphene/SiO_2/Si structure. In order to directly observe the dynamic process of the electrochemical reaction at the interface of Cu and SiO_2, we also prepare a Cu/graphene/SiO_2/W structure to measure the cyclic voltammetry characteristics, where the bottom Si substrate is replaced with a W electrode, as shown in the cross-sectional SEM image in Figure 2C.

The mass transport process of the Cu species through the dielectrics includes both atom diffusion and ion drift.[29] The first one is the diffusion of Cu atoms at high temperature driven by the concentration gradient. Cu atoms are required to overcome the metallic bonding and be released from the metal matrix. The second one is the drift of Cu ions under an electric field. The Cu ions are generated by chemical or electrochemical reactions that happen at the Cu/SiO_2 interface. As Cu atoms cannot reduce the SiO_2 (Gibbs free energy of forming SiO_2 $\Delta_f G_m^0 = -455.2$ kJ/mol) to form Cu oxide ($\Delta_f G_m^0 = -155.2$ kJ/mol for CuO and -167.4 kJ/mol for Cu_2O), Cu atoms can be oxidized only by the residual of trace amounts of O_2 or moisture at the interface.

Figure 3A shows the representative Raman spectra of the graphene and GO before and after thermal stress. The intensity ratios of the D and G peak (I_D/I_G) and the 2D and G peak (I_{2D}/I_G) of graphene and GO before and after thermal stress are recorded in Figure 3B and C, respectively. Before the thermal stress,

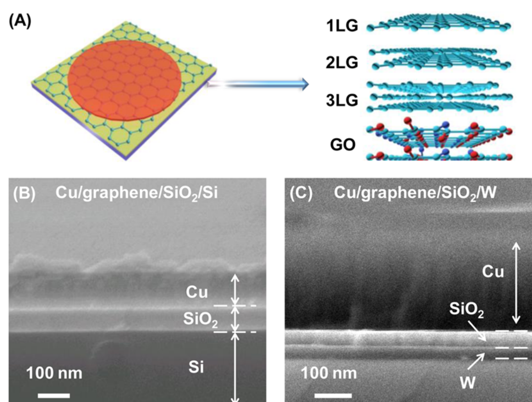

Figure 2. Test structures of the graphene barrier. (A) Schematic of Cu/barrier/SiO_2/Si structure. The barrier layer includes single-, double-, and triple-layer graphene and multiple-layered graphene oxide. Cross-sectional SEM images of (B) a Cu/graphene/SiO_2/Si structure and (C) a Cu/graphene/SiO_2/W structure.

the I_D/I_G for 1LG, 2LG, and 3LG samples is 0.037, 0.042, and 0.022, respectively, indicating that the pristine graphene is high-quality. We can roughly estimate the grain size of the graphene according to[30,31]

$$L_a(\text{nm}) = \frac{560}{E_{\text{laser}}^4}\left(\frac{I_D}{I_G}\right)^{-1} \quad (1)$$

where E_{laser} is the laser energy (eV) of the Raman spectroscopy. The grain sizes of the graphene samples in this work range from ~300 to ~700 nm. The I_{2D}/I_G (2.64 for 1LG, 1.11 for 2LG, and 0.48 for 3LG) indicates that the layer number of the graphene ranges from 1 to 3.[32] The high D peak and the large full width at half-maximum (fwhm) of the D and G peaks for the GO sample show the small grain size and many defects in the GO structure. The calculated grain size of the GO sample is about 16.50 nm, which is much smaller than that of the graphene samples. We then conducted the thermal stress test in a N_2 environment at 700 °C for 15 min and then etched the Cu thin film for spectroscopic characterization. As shown in Figure 3A−C, the I_D/I_G ratio of the graphene samples increases, and the I_{2D}/I_G of the graphene samples decreases after the thermal stress, indicating that the thermal stress induces structural defects in graphene. The defective sites can be the diffusion path for the mass transport of Cu species. For the GO sample, the D and G peak intensity becomes higher and the I_D/I_G becomes smaller. This indicates that the thermal stress reduces the GO sample.

Figure 3D shows the depth profiles of Cu species counts in the SiO_2 characterized by secondary ion mass spectroscopy (SIMS). Compared with the sample without the barrier layer, the 1LG sample only slightly decreases the total amount of Cu species that diffuse into the SiO_2. Double- and triple-layer graphene can effectively inhibit the diffusion of the Cu species. By integrating the Cu counts with respect to the depth in

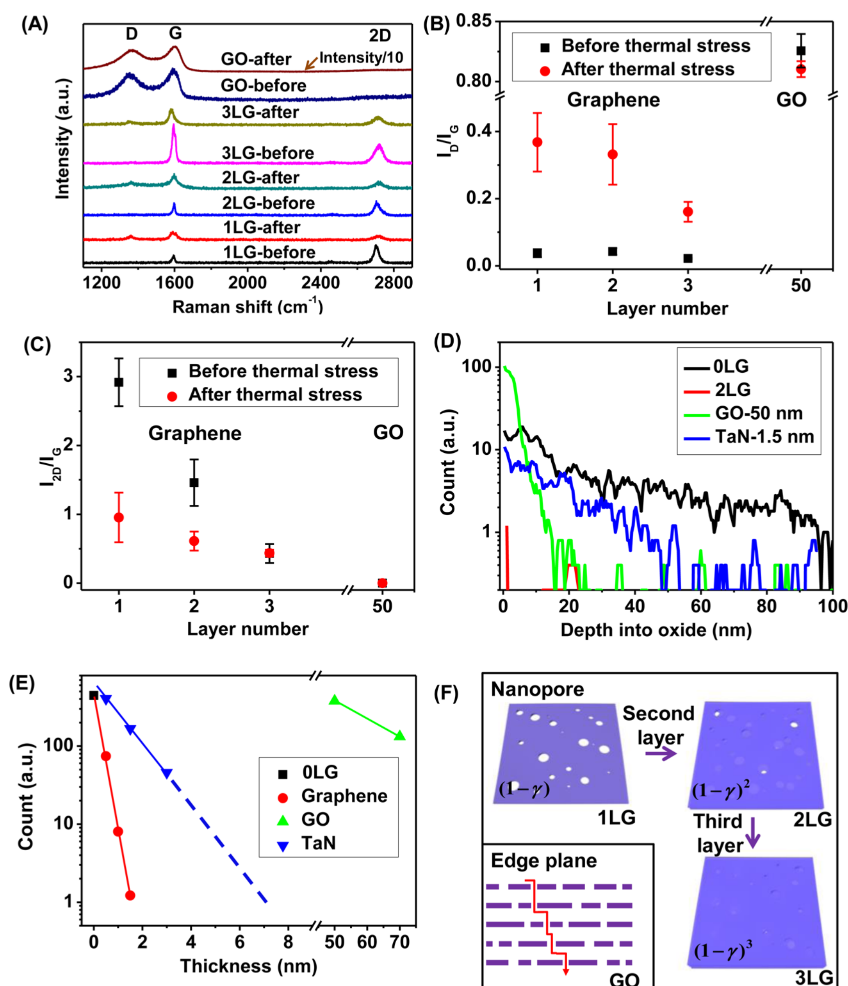

Figure 3. Thermal stress characterizations. (A) Raman spectra of single-, double-, and triple-layer graphene and graphene oxide (regarded as 1LG, 2LG, 3LG, GO) before and after thermal stress. The thermal stress condition is 700 °C for 15 min in a N_2 environment. (B) Intensity ratio of D and G Raman peaks of graphene before and after the thermal stress. (C) Intensity ratio of 2D and G Raman peaks of graphene before and after the thermal stress. (D) SIMS depth profile of Cu species into SiO_2 for the 0LG, 2LG, GO, and TaN samples. (E) Counts of the Cu species diffusing inside SiO_2 as a function of the thickness of the graphene, GO, and TaN barrier layer. (F) Schematic of the proposed diffusion path for graphene and the GO barrier layer.

SiO_2, we plot the total Cu amounts diffusing inside SiO_2 as a function of the thickness of the barrier layer in Figure 3E. Our results show that the Cu counts in the SiO_2 layer are 74.24 for 1LG, 8.02 for 2LG, and 1.22 for 3LG, which exponentially decrease with the increase of the number of graphene layers. In the thermal stress process, the majority of the Cu species injecting into the SiO_2 are Cu atoms. We define the coverage γ of single-layer graphene as the fraction of the area covered by graphene in the whole surface. As we stacked the monolayer graphene layer by layer, the locations of grain boundaries and defects in each layer are independent and can be covered by another adjacent graphene layer, as illustrated in Figure 3F. Therefore, the total coverage of the n-layer graphene can be expressed as $1 - (1 - \gamma)^n$. Accordingly, the porosity of the MLG can be described as $(1 - \gamma)^n$, an exponential decay parameter. The fitted line in Figure 3E matches well with the exponential decay trend. We can deduce that the porosity of single-layered graphene is about 2%. As illustrated by the DFT calculation, the migration path of the Cu species through MLG is the overlapped defects larger than the 0.25 nm^2. It is worth noting that the MLG directly grown on Ni or Cu foil is different from that fabricated using layer-by-layer transfer of monolayer graphene. The MLG grown on Ni or Cu foils is usually from the same nucleation site,[33,34] and the defects and grain boundaries in this kind of MLG are very likely to be overlapped.[19,20] However, the MLG using layer-by-layer transfer of monolayer graphene reduces the coincidences of the defects in different graphene layers and greatly enhances the barrier performance.

We also compared the SIMS characterization results with the sample with a TaN layer, a commonly used Cu interconnect barrier material in industry. The TaN thin film is difficult to keep in a continuous form at subnanoscale. The "nominal" thickness was measured based on the quartz crystal monitor inside the sputtering system. The diffusing Cu counts of the sample with

the TaN barrier also decayed exponentially with the "nominal" thickness of the TaN layer. The intercept with the thickness axis in Figure 3E indicates the "critical" thickness of the barrier layer for completely blocking the Cu migration. The estimated "critical" thicknesses for graphene and the TaN barrier are 1.5 and 7.5 nm, respectively. On the basis of the SIMS characterizations, the graphene layer shows much better barrier performance than the TaN with similar thickness. Zhao *et al.* used 3 nm thick TaN thin film as a barrier layer and found that the barrier fails above 500 °C thermal stress because the subnanoscale TaN thin film formed by vapor deposition is nonuniform.[35] In addition, the graphene barrier layer has a low sheet resistance compared with TaN. Figure S1 shows the sheet resistance as a function of the barrier thickness. Below 10 nm thickness, the sheet resistance of graphene is 4 orders of magnitude lower than that of TaN. This can reduce the resistance−capacitance time delay of the interconnect structure.

Remarkably, the count of the Cu species diffusing into SiO_2 in the sample with the GO barrier is close to that in the 0LG sample, although the thickness of the GO barrier is up to 50 nm, showing ultimately permeability to the Cu species. The GO nanoflakes with lateral sizes of tens of nanometers are rich with edge planes and pile up together to form a lamellar thin film. Although some Cu atoms may adsorb at the edge sites, the steric hindrance effect is not a dominant factor for the mass transport due to the relatively large distance between adjacent nanoflakes, as indicated by our DFT calculations. In addition, the interlayer distance of the GO sample prepared by a modified Hummers' method is over 0.86 nm, larger than distance (∼0.54 nm) of the MLG sample by layer-by-layer transfer.[36] For the interlayer distance smaller than 0.7 nm, graphene can block the intercalation of atoms and molecules.[37,38] The large interlayer distance in the GO sample can facilitate the Cu migration through the interlayer, as schematically shown in Figure 3F. Compared with few-layered graphene, the thick GO membrane (50 nm) still shows poor barrier performance.

According to Fick's diffusion law, we can know the Cu concentration as a function of the depth x after the thermal stress with a period of t:

$$\rho(x,t) = \rho_s\left(1 - \frac{2}{\sqrt{\pi}}\int_0^{x/2\sqrt{Dt}} e^{-t^2}\,dt\right) \qquad (2)$$

where $\sqrt{Dt}$ is the characteristic diffusion depth, D is the diffusivity, t is the diffusion time, and ρ_s is the surface concentration. We can fit the Cu counts with this equation and extract the effective diffusion depth. Our results show that the diffusion depths are 30.38 nm for the 0LG sample, 22.72 nm for the TaN (1.5 nm "nominal" thickness) sample, 14.36 nm for the GO (50 nm thickness) sample, and 2.95 nm for the 2LG sample. Although the total Cu count diffusing inside oxide in the GO sample is similar to that in the 0LG sample and is larger than that in the TaN sample, the effective diffusion depth of the GO sample is the smallest among the three samples. This indicates that the interlayer of the GO sample provides a large space for storing Cu species. Ogata *et al.* reported that Cu atoms can be oxidized by the GO barrier.[39] The Cu ions and GO layer can form a coordination complex by adsorbing Cu ions with the functional groups.[28] At elevated temperatures, Cu ions desorb from the functional groups and diffuse along the edge plane.

Bias Thermal Stress. A major difference between the thermal stress and the electrical stress is the migration species, where Cu atom diffusion is dominant in the thermal stress, and Cu ion drift due to the electric field plays a major role in the bias thermal stress (BTS). The equilibrium capacitance−voltage ($C-V$) measurement allows us to subtly detect the charge distribution in the SiO_2 layer by comparing the flatband voltage shift.[40] The relationship between the flatband voltage and the charge in the SiO_2 can be expressed as[40]

$$\Delta V_{FB} = -\frac{1}{C_0}\int_0^{d_0} \frac{x\rho(x)}{d_0}\,dx \qquad (3)$$

where $\rho(x)$ is the charge density at the distance x from the Cu/SiO_2 interface, d_0 is the thickness of the SiO_2 layer, and C_0 is the capacitance of the oxide layer per unit area. The quantity of the charge Q in the oxide layer can be expressed as $C_0\Delta V_{FB}$. As shown in Figure 4A, the initial flatband voltage (V^i_{FB}) is the work function difference between the metal and Si. When there are Cu ions in the oxide layer, it will electrostatically induce the electrons at the SiO_2/Si interfaces, as shown in Figure 4B and C. In order to neutralize the charge at the SiO_2/Si interface, a negative flatband voltage (V_{FB}) is required to be applied on the metal (Figure 4D). Thus, we can accurately detect the charge inside the oxide by measuring V^i_{FB}. We performed the BTS test on a Cu/barrier/SiO_2 (100 nm)/Si sample at 150 °C. The stressing electric field is relatively low, from 0.5 to 1.5 MV/cm, which ensures that the leakage current is caused by Cu ion drift instead of dielectric failure. Figure 4E shows the normalized $C-V$ curves of the different samples after an 8 min BTS under the electric field of 1 MV/cm. The charge-induced flatband voltage shifts are −2.05 and −0.4 V for the 0LG and 1LG samples, while we cannot observe an obvious shift of the flatband voltage for the samples with the 2LG, 3LG, and GO barrier layers.

Figure 4F shows the calculated counts of the drifted Cu ions in the SiO_2 as a function of the thickness of the barrier layer after 8 min BTS at 150 °C. When the electric field increases from 1 MV/cm to 1.5 MV/cm, the ion counts in the SiO_2 increase accordingly. Our results showed that the 1LG sample can only partially inhibit the ion drift and the 2LG and 3LG samples can effectively suppress the ion drift. Although the thickness of the GO sample is much larger than other samples, the

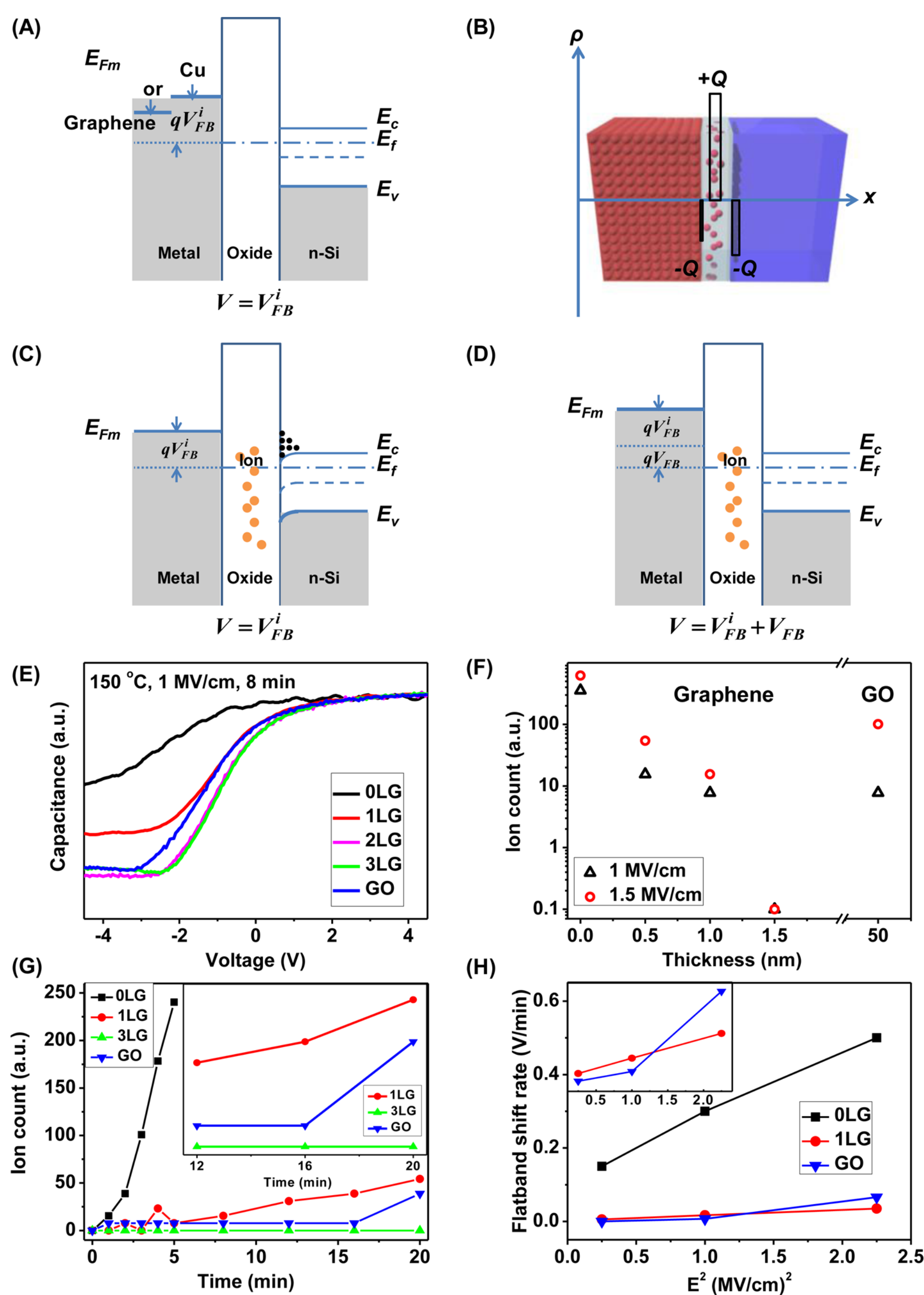

Figure 4. Bias thermal stress characterizations. (A) Energy band diagram of the metal-oxide–semiconductor structure without metal charges. (B) Diagram of metal charges in the oxide and the induced charges at the interface. (C) Bent band structure induced by metal charge in the oxide. (D) Flatband condition when applying a negative voltage on the metal. (E) Capacitance–voltage curve of different samples after 1 MV/cm electric field stress at 150 °C for 8 min. (F) Calculated Cu ion count as a function of the barrier thickness after 1 MV/cm and 1.5 MV/cm electric field stress at 150 °C for 8 min. (G) Calculated Cu ion count after 1 MV/cm electric field stress at 150 °C as a function of stress time. Inset shows the magnified curves for the 1LG, 3LG, and GO samples. (H) Relationship between the flatband shift rate and the square of the electric field. The inset shows the magnified curves for 1LG and GO samples.

barrier performance is weaker. In the BTS condition, Cu atoms have to be oxidized into ions and then drifted under the electric field. The Cu ions are generated from the chemical reactions at the Cu/SiO_2 interface, where a few species (O_2 or H_2O) adsorb on the SiO_2 surface. The continuous two-dimensional characteristics and chemical inertness of the graphene barrier make the Cu/SiO_2 interface more chemically stable. Hence, the presence of the graphene barrier not only retards the mass transport of Cu species through the graphene but also inhibits the chemical reactions at the interface. Different from the thermal stressing, we can observe that the ion count drifting into the SiO_2 is not exponentially decayed as a function of the thickness of the barrier layer. We tentatively attribute this trend to the two steps in the BTS process: Cu oxidation and Cu ion drift under an electric field.

We further performed a time-dependent $C-V$ test and observed the dynamics of the Cu ion drift during the BTS. Figure 4G shows the time evolution of the ion count at 150 °C and 1 MV/cm. Our results showed that the ion counts in the 0LG and 1LG samples are proportional to the stress time, while the ion quantity in the 3LG sample was kept below the detection limit. The time derivative of eq 3 is

$$\frac{d\Delta V_{FB}(t)}{dt} = -\frac{1}{C_0}\int_0^{d_0} \frac{x}{d_0}\frac{\partial \rho(x,t)}{\partial t}dx \quad (4)$$

Before the ions accumulate at the interface of SiO_2/Si, the boundary condition is $\rho(d_0, t) = 0$ and $J(d_0, t) = 0$, where $J(d_0, t)$ is the diffusion flux at time t and at the interface of SiO_2/Si. By applying Gauss's law, eq 4 can be written as[41]

$$\frac{d\Delta V_{FB}}{dt} = -\frac{D}{C_0 d_0}\rho_m(0) - \frac{2qD}{kT}E_0^2 \quad (5)$$

where D is the Cu ion diffusivity in the SiO_2 film, $\rho_m(0)$ is the maximum ion density at the interface of Cu/SiO_2, q is the unit charge, k is the Boltzmann constant, T is the temperature, and E_0 is the applied electric field. From eq 5, we can see that the rate of the flatband voltage shift is proportional to the square of the electric field. Figure 4H shows the flatband voltage shift rate as a function of the square of the electric field for the 0LG, 1LG, and GO samples. The effective diffusivity D can be extracted from the slope of the line, and the maximum ion concentration $\rho_m(0)$ at the interface of Cu/SiO_2 can be calculated from the intercept. The calculated results showed that the effective diffusivities of the Cu ions in the 0LG and 1LG sample are 3.7×10^{-21} and 3.1×10^{-22} m^2/s, respectively. The calculated Cu ion diffusivity into SiO_2 without the barrier in our work is comparable with a previous report.[42] The maximum Cu ion density $\rho_m(0)$ at the Cu/SiO_2 interface is 1.36×10^{-2} and 2.83×10^{-3} mol/cm^3 in the 0LG sample and 1LG sample, respectively. The ion density in the 1LG sample is reduced by 4.81 times than that of the 0LG sample. On the basis of these results, we can see that the graphene barrier significantly decreases the Cu ion density at the interface. The generation of the Cu ions at the interface becomes a rate-limiting factor during the BTS process.

The inset of Figure 4G shows the Cu ion counts in the SiO_2 as a function of the stressing time. Different from the sample with a graphene barrier, the Cu ion count in the GO sample shows an abrupt increase after 16 min BTS. At the initial period of 16 min, the Cu ion count in the GO sample was kept below the detection limit. In the subsequent 4 min, the ion drift increases dramatically and the ion count is similar to that in the 1LG sample after 20 min stress. When the electric field increases to 1.5 MV/cm, the abrupt change for the GO sample happens only after 1 min stress, and the ion count in the oxide is larger than that in the 1LG sample after 8 min stress, as shown in Figure S2. The inset of Figure 4H shows the relationship between the flatband voltage shift rate and the square of the applied electric field for 1LG and GO samples. Compared with the graphene sample, the GO sample shows a threshold voltage for Cu ion transport. We attribute these phenomena to the adsorption of Cu ions on the GO layers and classify the migration mechanisms into two types. First, Cu ions and the functional groups of the GO samples can form a coordination complex, and the Cu ions are trapped in the GO layer.[28] The functional groups are rich in the edge sites of GO nanoflakes and provide a strong interaction with the Cu ion. Second, the cation$-\pi$ interaction between Cu ions and the GO contributes to the accumulation and the fast transport of Cu ions in the interlayer under the drive of the electric field.[26] Under a low electric field, the Cu ions are trapped in the functional groups of the GO. However, a small amount of Cu ions may still migrate through the edge plane and interlayers of the GO. When the electric field is large enough to desorb the Cu ions from the functional groups, large amounts of Cu ions diffuse into the interlayer and translocate fast under the drive of the electric field.

Cyclic Voltammetry. To probe the Cu ion generation at the metal/dielectric interface, we prepare a Cu/interlayer/SiO_2/W structure, as shown in Figure 5A, which is intrinsically a solid-state electrochemical system. We conducted cyclic voltammetry measurements to examine the electrochemical reaction at the interface between Cu and SiO_2, as shown in Figure 5B. The compliance current is set as 1 μA to avoid Cu filament formation inside the oxide, and the voltage sweep rate is 250 mV/s. For the 0LG sample, the current increases dramatically at 0.375 V, indicating that the Cu atoms are oxidized into Cu ions and drift into the oxide layer under the electric field. After reaching the vertex voltage (0.500 V), the voltage sweep direction is reversed. Three current peaks can be observed, at 0.475, 0.375 and 0.300 V, corresponding to the oxidation of the Cu atoms to the Cu ions. During the negative voltage sweep, two reduction peaks can be observed, at -0.050 and -0.465 V. We also observe one oxidation peak, at -0.45 V, due to the oxidation of the Cu atoms that were previously reduced at the W electrode. For the 1LG sample, the onset potential of oxidation is 0.475 V, larger than that of the 0LG sample. Because of the presence of a graphene barrier, the concentration of the Cu ions at the graphene/SiO_2 interface increases slowly. Hence, the onset voltage shifts more positively. During the reverse voltage sweep, three oxidation peaks, at 0.475, 0.375, and 0.300 V, and one reduction peak, at -0.050 V, can be observed. Although the current is reduced by the presence of single-layer graphene, the generated Cu ions can still penetrate through the defective sites of the graphene barrier. For the 2LG and 3LG samples, the current is

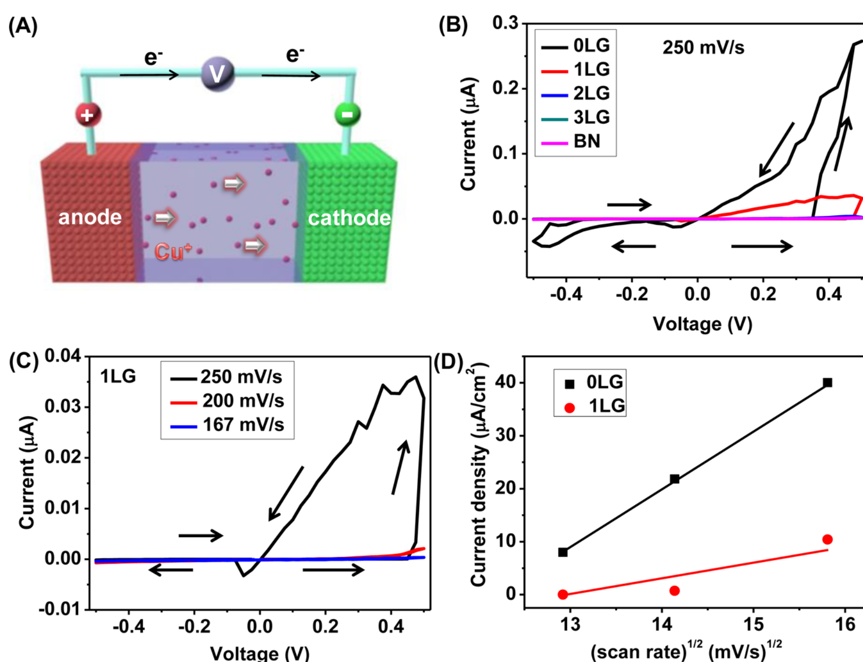

Figure 5. Cyclic voltammetry characterization. (A) Schematic of Cu/SiO_2/W structure and the electrochemical reaction at the interface. (B) Current–voltage curves of Cu/interlayer/SiO_2/W structure at a scan rate of 250 mV/s. Interlayer contains 0LG, 1LG, 2LG, and h-BN, respectively. (C) Current–voltage curves of the Cu/1LG/SiO_2/W structure at different scan rates. (D) Plot of reduction peak current density with the square root of the voltage sweep rate.

100 times smaller than that of the 0LG samples. No oxidation/reduction currents can be observed for the 2LG and 3LG samples, indicating that the ion concentration at the interface is quite low and no obvious concentration gradient forms at the graphene/SiO_2 interface.

With the 2LG and 3LG barrier, the Cu ion drift inside SiO_2 is significantly reduced. The SiO_2 is also an insulator for the electron that is injected from the cathode. The generated Cu ion cannot be reduced by the injected electrons. Thus, the electrochemical reaction of the Cu oxidation is greatly inhibited, and the Cu ion concentration at the interface is significantly reduced. Although graphene has high in-plane electrical conductivity, it has weak coupling with ions and low conductivity in the vertical direction.[43] The inhibition effect of Cu ion generation with a graphene barrier is close to that by an insulator. Figure 5B shows the cyclic voltammetry measurement with few-layered hexagonal boron nitride (9 nm) as the barrier layer. The electrochemical redox current is quite low, similar to that in the 3LG sample. The cyclic voltammetry measurements also show that the oxidation of the Cu atom is a rate-limiting factor during the electrical stressing.

We conducted cyclic voltammetry measurement with different voltage sweep rates, as shown in Figure 5C. The oxidation/reduction current peaks increase with the sweep rate. At room temperature, the relationship between the scan rate and the peak current can be described according to the Randles–Sevcik equation:[44,45]

$$j_p = 2.686 \times 10^5 n^{3/2} D^{1/2} \rho v^{1/2} \quad (6)$$

where j_p is the current density of the redox peak in A/cm^2, n is the number of electrons transferred in the redox event, D is the diffusion coefficient in cm^2/s, ρ is the ion concentration in mol/cm^3, and v is the scan rate in V/s. We can see that j_p is linearly proportional to $v^{1/2}$. Figure 5D shows the reduction peak current density of the 0LG and 1LG samples as a function of $v^{1/2}$. When the scan rate is 250 mV/s, we can estimate that the concentrations of the ions in the reductive reaction for the 0LG and 1LG sample are 8.32×10^{-6} and 2.16×10^{-6} mol/cm^3, respectively. The presence of single-layer graphene reduces the Cu ion concentration at the interface by 3.85 times. The effective diffusion coefficients for 0LG and 1LG samples are 2.54×10^{-12} and 2.49×10^{-12} m^2/s, respectively, showing negligible change.

CONCLUSIONS

In summary, we theoretically and experimentally study the mass transport mechanism of Cu species through the MLG barrier at the metal/dielectric interface. Our DFT calculation results suggest that the MLG barrier is highly resistant to Cu species migration except for the overlapped defects larger than an eight-atom vacancy (0.25 nm^2). Hence, we prepared the MLG barrier using layer-by-layer transfer of monolayer graphene to avoid the overlapped defects that usually exist in the MLG directly grown on Cu or Ni foils. On the basis of our experimental results, the "critical" thicknesses for completely retarding Cu species migration are 1.5 nm for the MLG and 7.5 nm for TaN, respectively, and the sheet resistance of the MLG is 4 orders of

magnitude lower than that of TaN. The BTS and cyclic voltammetry characterizations demonstrate that the Cu ion concentrations at the interface can be reduced by 4−5 times with the use of graphene. The graphene barrier can also inhibit the mass transport of Cu species through graphene and the electrochemical reactions at the Cu/SiO_2 interface simultaneously. These investigations show that graphene is a promising candidate for a next-generation barrier of a Cu interconnect and opens up the possibilities of controllable mass transport in solid-state electrolyte devices with a graphene barrier.

METHODS

The calculations of self-consistent fields were performed with Quantum Espresso.[46] The unit cell of single-layer graphene with no vacancy, monovacancy, divacancy, and eight-atom vacancy contains 32, 31, 30, and 72 carbon atoms, respectively. The convergence threshold on total energy and forces is 10^{-6} and 10^{-3} (in au). The kinetic energy cutoff for wave functions is 50 Ry, and the kinetic energy cutoff for charge density and potential is 200 Ry. In this work, we define the adsorption energy of a Cu atom on graphene as $E_{ad} = E_{ag} - E_a - E_g$, where E_{ag} is the total energy of one Cu atom adsorbed on a graphene supercell, E_a is the energy of an isolated Cu atom, and E_g is the energy of an isolated graphene supercell.

Thermal SiO_2 was grown on a 0.3−0.6 Ω·cm n-type Si (100) wafer. The thickness of the oxide layer is 100 nm. Cu was deposited onto the SiO_2 layer without pattern for thermal stressing test or was patterned with a shadow mask for the bias thermal stressing test. The diameter of the patterned Cu electrode is 1 mm. High-quality monolayer graphene was grown on Cu foil by the chemical vapor deposition method. A thin layer of poly(methyl methacrylate) (PMMA) was used as supporting layer to transfer graphene to other substrates. Double- and triple-layer graphene was stacked using a layer-by-layer transfer method. In the cyclic voltammetry test, the W electrode, SiO_2 layer, and Cu electrode were successively deposited onto the substrate by magnetron sputtering. The thickness of SiO_2 in the Cu/interlayer/SiO_2/W structure was 30 nm. The hexagonal boron nitride was grown on Cu foil by the chemical vapor deposition method. The Raman spectrum and the atomic force microscopy image of hexagonal boron nitride can be found in Figures S3 and S4 in the Supporting Information.

The cross-sectional images of the test structures were performed using a JEOL JSM-633F field emission SEM. Raman spectroscopy (Horiba HR800) with an excitation wavelength of 488 nm was used to study the atomic vibration of graphene. TOF-SIMS was used to characterize the Cu count in the SiO_2. The $C-V$ test was performed with an Agilent 4294A precision impedance analyzer. The cyclic voltammetry test was performed with a Keithley 2400 sourcemeter.

Conflict of Interest: The authors declare no competing financial interest.

Supporting Information Available: The sheet resistance as a function of thickness, capacitance−voltage curve, Raman spectrum, and atomic force microscope image of BN. This material is available free of charge *via* the Internet at http://pubs.acs.org.

Acknowledgment. We acknowledge partial financial support from the National Natural Science Foundation of China (grant number 61302045) and the Hong Kong Polytechnic University (grant numbers G-UA51, G-YN02, and G-UC72).

REFERENCES AND NOTES

1. Cho, J.; Gungor, M.; Maroudas, D. Effects of Electromigration-Induced Void Dynamics on the Evolution of Electrical Resistance in Metallic Interconnect Lines. *Appl. Phys. Lett.* **2005**, *86*, 241905.
2. Cho, J.; Gungor, M.; Maroudas, D. Current-Driven Interactions between Voids in Metallic Interconnect Lines and Their Effects on Line Electrical Resistance. *Appl. Phys. Lett.* **2006**, *88*, 221905.
3. Chai, Y.; Chan, P. C. H.; Fu, Y.; Chuang, Y. C.; Liu, C. Y. Electromigration Studies of Cu/Carbon Nanotube Composite Interconnects Using Blech Structure. *IEEE Electron Device Lett.* **2008**, *29*, 1001–1003.
4. Chai, Y.; Chan, P. C. H. *High Electromigration-Resistant Copper/Carbon Nanotube Composite for Interconnect Application*; International Electron Devices Meeting; 2008; p 610.
5. Chen, F.; Shinosky, M. Addressing Cu/Low-*k* Dielectric TDDB-Reliability Challenges for Advanced CMOS Technologies. *IEEE Trans. Electron Devices* **2009**, *56*, 2–12.
6. Yang, C.-C.; Li, B.; Baumann, F. H.; Li, J.; Edelstein, D.; Rosenberg, R. Microstructure Modulation in Copper Interconnects. *IEEE Electron Device Lett.* **2014**, *35*, 572–574.
7. International Technology Roadmap for Semiconductor. www.itrs.net.
8. Araujo, R. A.; Yoon, J.; Zhang, X.; Wang, H. Cubic TaN Diffusion Barrier for Cu Interconnects Using an Ultra-Thin TiN Seed Layer. *Thin Solid Films* **2008**, *516*, 5103–5106.
9. Bunch, J. S.; Verbridge, S. S.; Alden, J. S.; van der Zande, A. M.; Parpia, J. M.; Craighead, H. G.; McEuen, P. L. Impermeable Atomic Membranes from Graphene Sheets. *Nano Lett.* **2008**, *8*, 2458–2462.
10. Berry, V. Impermeability of Graphene and Its Applications. *Carbon* **2013**, *62*, 1–10.
11. Zhao, Y.; Xie, Y.; Liu, Z.; Wang, X.; Chai, Y.; Yan, F. Two-Dimensional Material Membranes: An Emerging Platform for Controllable Mass Transport Applications. *Small* **2014**, 10.1002/smll.201401549.
12. Leenaerts, O.; Partoens, B.; Peeters, F. M. Graphene: A Perfect Nanoballoon. *Appl. Phys. Lett.* **2008**, *93*, 193107.
13. Mohanty, N.; Fahrenholtz, M.; Nagaraja, A.; Boyle, D.; Berry, V. Impermeable Graphenic Encasement of Bacteria. *Nano Lett.* **2011**, *11*, 1270–1275.
14. Yuk, J. M.; Park, J.; Ercius, P.; Kim, K.; Hellebusch, D. J.; Crommie, M. F.; Lee, J. Y.; Zettl, A.; Alivisatos, A. P. High-Resolution EM of Colloidal Nanocrystal Growth Using Graphene Liquid Cells. *Science* **2012**, *336*, 61–64.
15. Zhao, Y.; Xie, Y.; Hui, Y. Y.; Tang, L.; Jie, W.; Jiang, Y.; Xu, L.; Lau, S. P.; Chai, Y. Highly Impermeable and Transparent Graphene as an Ultra-Thin Protection Barrier for Ag Thin Films. *J. Mater. Chem. C* **2013**, *1*, 4956–4961.
16. Hsieh, Y.; Hofmann, M.; Chang, K.; Jhu, J. G.; Li, Y.; Chen, K. Y.; Yang, C. C.; Chang, W.; Chen, L. Complete Corrosion Inhibition through Graphene Defect Passivation. *ACS Nano* **2014**, *8*, 443–448.
17. Zhao, Y.; Xie, Y.; Bao, Z.; Tsang, Y. H.; Xie, L.; Chai, Y. Enhanced SERS Stability of R6G Molecules with Monolayer Graphene. *J. Phys. Chem. C* **2014**, *118*, 11827–11832.
18. Kim, H.; Lee, C.; Kim, J.; Ren, F.; Pearton, S. J. Graphene as a Diffusion Barrier for Al and Ni/Au Contacts on Silicon. *J. Vac. Sci. Technol. B* **2012**, *30*, 030602.
19. Nguyen, B.; Lin, J.; Perng, D. 1-nm-Thick Graphene Tri-Layer as the Ultimate Copper Diffusion Barrier. *Appl. Phys. Lett.* **2014**, *104*, 082105.
20. Hong, J.; Lee, S.; Lee, S.; Han, H.; Mahata, C.; Yeon, H.; Koo, B.; Kim, S.; Nam, T.; Byun, K.; *et al*. Graphene as an Atomically Thin Barrier to Cu Diffusion into Si. *Nanoscale* **2014**, *6*, 7503–7511.
21. Waser, R.; Aono, M. Nanoionics-Based Resistive Switching Memories. *Nat. Mater.* **2007**, *6*, 833–840.
22. Chai, Y.; Wu, Y.; Takei, K.; Chen, H.; Yu, S.; Chan, P. C. H.; Javey, A.; Wong, H.-P. Nanoscale Bipolar and Complementary

Resistive Switching Memory Based on Amorphous Carbon. *IEEE Trans. Electron Devices* **2011**, *58*, 3933–3939.
23. Prasai, D.; Tuberquia, J. C.; Harl, R. R.; Jennings, G. K.; Bolotin, K. I. Graphene: Corrosion-Inhibiting Coating. *ACS Nano* **2012**, *6*, 1102–1108.
24. Roy, S. S.; Arnold, M. S. Improving Graphene Diffusion Barriers *via* Stacking Multiple Layers and Grain Size Engineering. *Adv. Funct. Mater.* **2013**, *23*, 3638–3644.
25. Chan, K. T.; Neaton, J. B.; Cohen, M. L. First-Principles Study of Metal Adatom Adsorption on Graphene. *Phys. Rev. B* **2008**, *77*, 235430.
26. Joshi, R. K.; Carbone, P.; Wang, F. C.; Kravets, V. G.; Su, Y.; Grigorieva, I. V.; Wu, H. A.; Geim, A. K.; Nair, R. R. Precise and Ultrafast Molecular Sieving through Graphene Oxide Membranes. *Science* **2014**, *343*, 752–754.
27. Kim, H. W.; Yoon, H. W.; Yoon, S.; Yoo, B. M.; Ahn, B. K.; Cho, Y. H.; Shin, H. J.; Yang, H.; Paik, U.; Kwon, S.; *et al.* Selective Gas Transport through Few-Layered Graphene and Graphene Oxide Membranes. *Science* **2013**, *342*, 91–95.
28. Sun, P.; Zhu, M.; Wang, K.; Zhong, M.; Wei, J.; Wu, D.; Xu, Z.; Zhu, H. Selective Ion Penetration of Graphene Oxide Membranes. *ACS Nano* **2013**, *7*, 428–437.
29. Kaloyeros, A.; Eisenbraun, E. Ultrathin Diffusion Barriers/Liners for Gigascale Copper Metallization. *Annu. Rev. Mater. Sci.* **2000**, *30*, 363–385.
30. Ferrari, A.; Robertson, J. Interpretation of Raman Spectra of Disordered and Amorphous Carbon. *Phys. Rev. B* **2000**, *61*, 14095–14107.
31. Pimenta, M. A.; Dresselhaus, G.; Dresselhaus, M. S.; Cancado, L. G.; Jorio, A.; Saito, R. Studying Disorder in Graphite-Based Systems by Raman Spectroscopy. *Phys. Chem. Chem. Phys.* **2007**, *9*, 1276–1291.
32. Ferrari, A. C.; Basko, D. M. Raman Spectroscopy as a Versatile Tool for Studying the Properties of Graphene. *Nat. Nanotechnol.* **2013**, *8*, 235–246.
33. Chae, S. J.; Guenes, F.; Kim, K. K.; Kim, E. S.; Han, G. H.; Kim, S. M.; Shin, H.; Yoon, S.; Choi, J.; Park, M. H.; *et al.* Synthesis of Large-Area Graphene Layers on Poly-Nickel Substrate by Chemical Vapor Deposition: Wrinkle Formation. *Adv. Mater.* **2009**, *21*, 2328–2333.
34. Wofford, J. M.; Nie, S.; McCarty, K. F.; Bartelt, N. C.; Dubon, O. D. Graphene Islands on Cu Foils: The Interplay between Shape, Orientation, and Defects. *Nano Lett.* **2010**, *10*, 4890–4896.
35. Zhao, C.; Toekei, Z.; Haider, A.; Demuynck, S. Failure Mechanisms of PVD Ta and ALD TaN Barrier Layers for Cu Contact Applications. *Microelectron. Eng.* **2007**, *84*, 2669–2674.
36. Some, S.; Kim, Y.; Yoon, Y.; Yoo, H.; Lee, S.; Park, Y.; Lee, H. High-Quality Reduced Graphene Oxide by a Dual-Function Chemical Reduction and Healing Process. *Sci. Rep.* **2013**, *3*, 1929.
37. Nair, R. R.; Wu, H. A.; Jayaram, P. N.; Grigorieva, I. V.; Geim, A. K. Unimpeded Permeation of Water through Helium-Leak−Tight Graphene-Based Membranes. *Science* **2012**, *335*, 442–444.
38. Liu, Z.; Li, J.; Yan, F. Package-Free Flexible Organic Solar Cells with Graphene Top Electrodes. *Adv. Mater.* **2013**, *25*, 4296–4301.
39. Ogata, C.; Koinuma, M.; Hatakeyama, K.; Tateishi, H.; Asrori, M. Z.; Taniguchi, T.; Funatsu, A.; Matsumoto, Y. Metal Permeation into Multi-layered Graphene Oxide. *Sci. Rep.* **2014**, *4*, 3647.
40. Fisher, I.; Eizenberg, M. Copper Ion Diffusion in Porous and Nonporous SiO_2-Based Dielectrics Using Bias Thermal Stress and Thermal Stress Tests. *Thin Solid Films* **2008**, *516*, 4111–4121.
41. He, M.; Ou, Y.; Wang, P.; Lu, T. Kinetics of Ta Ions Penetration into Porous Low-*k* Dielectrics under Bias-Temperature Stress. *Appl. Phys. Lett.* **2010**, *96*, 222901.
42. Shachamdiamand, Y.; Dedhia, A.; Hoffstetter, D.; Oldham, W. Copper Transport in Thermal SiO_2. *J. Electrochem. Soc.* **1993**, *140*, 2427–2432.
43. Garaj, S.; Hubbard, W.; Reina, A.; Kong, J.; Branton, D.; Golovchenko, J. A. Graphene as a Subnanometre Trans-Electrode Membrane. *Nature* **2010**, *467*, 190–193.
44. Zanello, P. *Inorganic Electrochemistry: Theory, Practice and Application*; The Royal Society of Chemistry: Cambridge, 2003; pp 14−15.
45. Tappertzhofen, S.; Menzel, S.; Valov, I.; Waser, R. Redox Processes in Silicon Dioxide Thin Films Using Copper Microelectrodes. *Appl. Phys. Lett.* **2011**, *99*, 203103.
46. Giannozzi, P.; Baroni, S.; Bonini, N.; Calandra, M.; Car, R.; Cavazzoni, C.; Ceresoli, D.; Chiarotti, G. L.; Cococcioni, M.; Dabo, I.; *et al.* QUANTUM ESPRESSO: a Modular and Open-Source Software Project for Quantum Simulations of Materials. *J. Phys.: Condens. Matter* **2009**, *21*, 395502.